

# Instabilities of Rotating Jets

by

Russell Zahniser

Submitted to the Department of Physics  
in partial fulfillment of the requirements for the degree of

Bachelor of Science in Physics

at the

MASSACHUSETTS INSTITUTE OF TECHNOLOGY

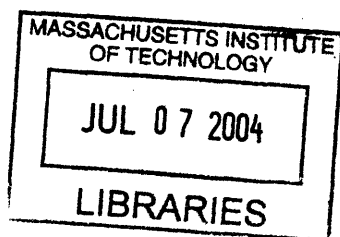
June 2004

© Massachusetts Institute of Technology 2004. All rights reserved.

Author .....  
Department of Physics  
May 17, 2004

Certified by .....  
John Bush  
Associate Professor  
Thesis Supervisor

Accepted by .....  
David Pritchard  
Thesis Coordinator



ARCHIVES



# Instabilities of Rotating Jets

by

Russell Zahniser

Submitted to the Department of Physics  
on May 7, 2004, in partial fulfillment of the  
requirements for the degree of  
Bachelor of Science in Physics

## Abstract

When a jet of water is in free fall, it rapidly breaks up into drops, since a cylinder of water is unstable. This and other problems involving the form of a volume of water bound by surface tension have yielded a wealth of theoretical and experimental results, and given insight into such phenomena as the shape of the Earth. Particularly interesting behaviors tend to emerge when the fluid in question is rotating; a drop may, for example, form a toroidal or ellipsoidal shape or even stretch out into some multi-lobed, non-axisymmetric form. In this paper, we investigate the properties of a rotating jet of water, and determine what regime of the parameter space are dominated by the various forms of instability. This is both predicted theoretically and demonstrated to be accurate experimentally.

If we watch a jet of water as the rotation rate is gradually increased from zero, the drop size will start shrinking gradually, and then suddenly, rather than a single row of drops, we will see the jet breaking up into two-lobed, bar shaped forms, like the rung of a ladder. The point at which this transition occurs is characterized in terms of the rotational Bond number,  $B_0 = \frac{\rho\Omega^2 R_0^3}{\sigma}$ . The critical  $B_0$  may be as low as 6, if there is a strong bias imparted by vibration of the table at an appropriate frequency, but for a perfectly quiescent rotating jet the second mode does not become dominant until a higher  $B_0$ . As the rotation rate is increased above this, the instability grows gradually more dramatic, and eventually the two lobes of each drop are breaking apart and flying outward. Then a transition to a third mode will occur, with three lobes in each drop; this is possible from a  $B_0$  of 12, and dominant above a  $B_0$  slightly higher than that. In general, mode  $m$  may occur whenever  $B_0 > m(m + 1)$

Thesis Supervisor: John Bush

Title: Associate Professor



## Acknowledgments

In preparing this paper and the described experiment, I was working with Nikos Savva and Professor John Bush. We also were helped by Andy Gallant in the machine shop, and Professor Harvey Greenspan.



# Contents

<b>1</b>	<b>Introduction</b>	<b>11</b>
<b>2</b>	<b>Background</b>	<b>13</b>
2.1	Jet Breakup . . . . .	13
2.2	Prior work . . . . .	14
2.3	Governing equations . . . . .	16
2.3.1	Boundary conditions . . . . .	20
2.4	Consequences of Theory . . . . .	22
<b>3</b>	<b>Experiment</b>	<b>25</b>
<b>4</b>	<b>Results</b>	<b>31</b>
4.1	Experimental Results . . . . .	31
4.2	Contributions . . . . .	32





# List of Figures

2-1	The types of perturbation we use to detect instability to modes 0, 2, 3 and 4. The size of the perturbation is exaggerated greatly so that it will be visible.	17
2-2	The dispersion relationship between wavelength and wave speed, for various values of $B_0$ . Wavelengths above $2\pi$ are not real traveling waves. Note that for some fixed value of $U$ , that is, a fixed position on the jet, the stationary wavelength grows smaller the bigger the rotation rate $\Omega$ .	23
3-1	The experimental setup. A pump feeds water from the large reservoir into a small drum which can be rotated reliably at any speed from 1 to 18 Hz. This water then exits through any of a number of interchangeable nozzles. The jet can be seen more clearly using a strobe light.	26
3-2	A sequence showing the water jet breakup as rotation rate increases, for a jet radius $R_0 = .95\text{cm}$ . Note that the mode 0 instability first starts to grow more rapidly and to segment off smaller, ellipsoidal drops	28
3-3	As the rotation rate increases, mode appears (middle) and grows progressively more unstable. Jet radius here is still $R_0 = .95\text{cm}$ . The individual drops, rather than consolidating back into a drop under the influence of surface tension as their rotation rate slows, instead are torn apart into two main drops, usually leaving some daughter drops as well where the connecting bar was.	29
3-4	At fairly high rotation rates, mode 2 instabilities develop immediately and the jet breaks up almost as soon as it leaves the nozzle. Mode 3 may be visible in the final picture.	30



# Chapter 1

## Introduction

In fluid dynamics, questions of stability are of fundamental importance. If a particular type of fluid flow exists in nature, it has to be both valid according to the relevant governing equations, and stable. One can readily write some equations showing how water from a tap falls in a nice laminar stream, gradually narrowing as it speeds up, and those equations will be perfectly valid [3]; however, you will never see this in real life, because any real cylinder of water is unstable and will break up into drops.

In this paper, we investigate essentially this same problem, with an added twist: we consider water jets that are rotating. The instabilities thus produced are much more dramatic and asymmetric than simple drop pinch-off. Prior work has led us to believe that we may, for example, see drops split off into two lobes connected by a narrow bar, or even three or four such lobes.

The behavior the axisymmetric mode under rotation has been quantitatively investigated [11], and a qualitative description of the second mode has been given [1], but this will be the first comprehensive and qualitative description of the different modes and the regimes in which they occur.

In preparing this paper and the described experiment, I was working with Nikos Savva and Professor John Bush in the applied math department. We also were helped by Andy Gallant in the machine shop, and Professor Harvey Greenspan. It was, for the most part, my job to build the experimental apparatus and get it to work, whereas Nikos worked on the theoretical aspects of the problem.



# Chapter 2

## Background

### 2.1 Jet Breakup

When a jet of fluid is in free fall, it must eventually break up into individual drops. This is inevitable because, as Plateau first demonstrated experimentally in 1873, any cylinder of fluid whose length is greater than its circumference is unstable to a perturbation that tends to break it up into drops [8]. The breakup phenomenon is a familiar one; it explains why a stream of water coming out of a faucet or shower head resolves quickly into individual drops. Rayleigh, in 1979, was the first to investigate this phenomenon rigorously as a stability problem, and he characterized the dependence of the breakup rate on the frequency of an original perturbation imposed on the ideal jet ([9], [10]). The minimum wavelength at which an unrotating jet can break up is equal to the circumference of a jet; wavelengths less than this belong to capillary waves.

Capillary waves are waves that travel along the surface of a jet, rather than growing in size. Rayleigh's equations revealed that a wave can either be a growing instability, or a traveling wave, but not both. The speed at which the wave travels is dependent on its wavelength. This leads to one effect where these surface waves are strikingly visible: when a thin jet is entering a fluid reservoir, the wave that happens to travel with a speed exactly equal to the jet speed at the point where the jet ends is then effectively stationary in the lab frame, and these waves build up to form a series of

corrugations visible at the bottom of the jet. This can be observed easily by adjusting a faucet to produce a stream only a few millimeters wide, and then blocking that stream with a finger. By moving your finger up and down, you can observe that the waves produced change in size as the velocity of the jet, increasing due to gravity the further down you block it, selects one particular wavelength to reinforce. The size of these waves can be fairly small, but the wavelength cannot be larger than the circumference of the jet, since at that point the transition is made to a stationary, growing instability ([3], [6]). We hope to discover theoretically and experimentally how this behavior extends into the case of a rotating jet.

## 2.2 Prior work

Our experiment is inspired in part by an experiment done by Gregory Balle, a student in Washington University's School of Oceanography. He discovered that a 1 cm jet of water of moderate size, exiting from a "bathtub" vortex in a tank and thus rotating rather quickly, would develop into a string of two-lobed, bar-shaped drops that look something like the rungs of a ladder. He hypothesized that this was a result of periodic breakup occurring on top of a two-lobed "base flow" as derived by Lamb (*Hydrodynamics*, chapter 12, [7]) for high rotation rates of a cylinder.

Our goal in extending his work is to quantify the phenomenon, and discover what other strange modes of instability may be lurking in the parameter space. Balle's experiment, in particular, did not attempt to measure or control the rotation rate or any other parameters of the jet. By introducing such controls, we hope to find the critical rotation rates at which different modes of instability occur, and show experimental results to be consistent with theoretical predictions.

We also had reason to believe that there might be even more exotic rotational modes available than the two-lobed one seen by Balle. Several investigations have been made into the instability of a rotating drop, and the possible forms it might take. For example, Elkins-Tanton et al. (2004, [5]) demonstrated that the odd shapes of splash-form tektites, which are formed from magma ejected from a meteorite impact,

correspond to the form of a rapidly moving and rotating drop that gradually cools. They discovered that tori, bars, and ellipsoids are all valid forms for a rotating drop to cool into, and were able to reproduce these forms out of spinning lumps of solder in the lab.

Brown and Scriven (1980, [2]) made a thorough investigation into the shape that a rotating drop will form if influenced merely by surface tension. They used a computer model to solve the energy-minimization problem at various rotation rates, and mapped out what instabilities might develop in various regimes of a parameter space in angular momentum and angular velocity. They discovered that the axisymmetric family of drop forms, where the sphere is squashed into an ellipsoid and then into a biconcave form like a red blood cell before breaking apart, are also unstable in various places along that progression to higher mode instabilities. For example, a rotating drop may suddenly develop a two lobed character, causing it to drop suddenly down in the angular velocity parameter while keeping high angular momentum. This can be envisioned as a bifurcation of a curve tracing out what possible angular velocity and angular momentum pairs might exist.

This last paper makes us strongly suspect that there will be instabilities of at least modes two through four accessible in our experiment. One of our goals is to produce a similar map showing which mode is most unstable, and thus the one that will appear, as a function of rotation rate. There are also several other parameters we could take into consideration if we wanted a more complex parameter space to map out.

There is also prior work suggesting that, even within a mode, there should be slight variations as we increase the rotation rate. Rutland and Jameson (1970, [11]) discovered that, in a very viscous liquid such as treacle, rotating a liquid stream greatly increases the rate of breakup. We might expect to observe, therefore, that within each mode, as we increase the rotation rate, full breakup into drops occurs closer to the nozzle of the jet, and the drops produced are smaller.

## 2.3 Governing equations

The theory summarized here is primarily the work of Nikos Savva [12]. The problem we are dealing with is that of a jet of water which, having been ejected out of some sort of an orifice, falls under the influence of gravity. If the jet is not rotating, the velocity of any particle in jet relative to those near to it will be zero. The pressure inside the jet will be a constant, greater than the atmospheric pressure by a small amount due to the force exerted by the tension of the surface. The Young-Laplace law tells us that this pressure differential is equal to the mean curvature times the surface tension, or  $\sigma \nabla \cdot \hat{n}$ ; for a cylinder, this is just  $\frac{\sigma}{R}$ .

If we then start to spin this jet, assuming a uniform, rigid-body rotation, we are introducing a velocity  $u_\phi = u_\theta = \Omega r$ . The centripetal acceleration here must be provided by a pressure gradient; hence:

$$\frac{\rho u_\phi^2}{r} = \frac{\partial p}{\partial r} \Rightarrow p_0(r) = \frac{1}{2} \rho \Omega^2 r^2 + p_{axis} \quad (2.1)$$

In order to determine the modes of instability to which the jet is unstable, we will impose a slight perturbation on it, setting  $R = R_0 + \tilde{R}$ , and observe the response. There are two types of behaviors we expect to have happen. First, as in Rayleigh's unrotating jet equations, we may seek axisymmetric travelling surface waves of phase velocity  $\frac{\omega}{k}$ , or growing surface waves of wave number  $k$ . This is expressed by a term whose instabilities are of the form  $e^{\omega t - ikz}$ , where  $\omega$  is either real, giving the growing pinch-off condition, or imaginary, giving the familiar form of a traveling wave. Second, there may be non-axially-symmetric instability. Any such instability would have to have some integer number  $m$  of identical lobes symmetrically distributed about the jet. This, then, adds a term  $e^{im(\Omega t - \phi)}$ . Putting this all together, we have

$$\tilde{R} = \epsilon e^{(\omega t - ikz) + im(\Omega t - \phi)} \quad (2.2)$$



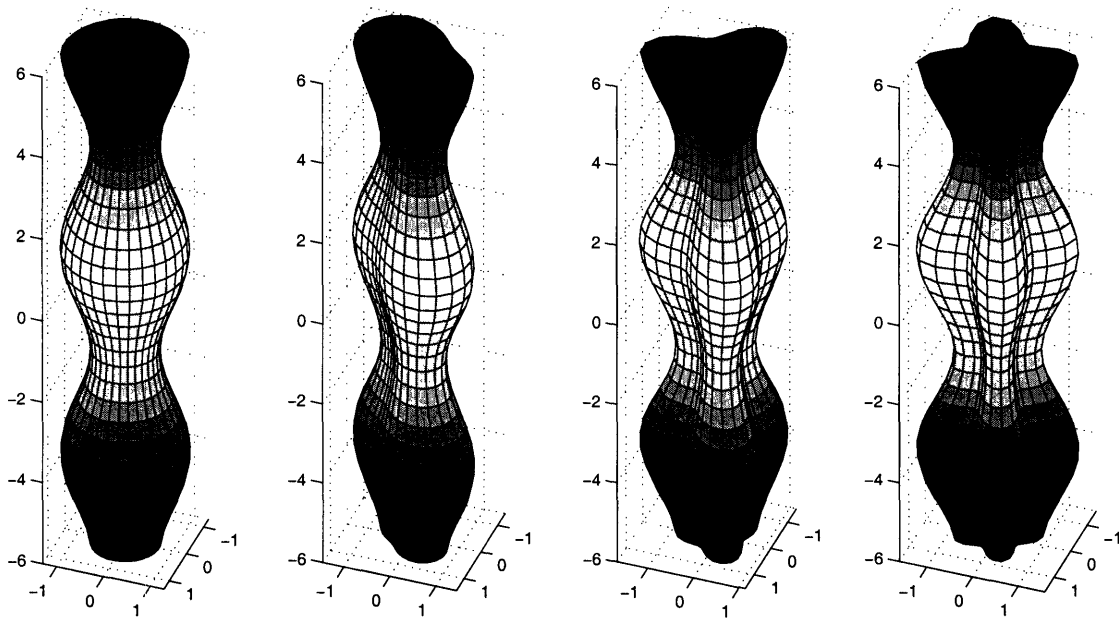


Figure 2-1: The types of perturbation we use to detect instability to modes 0, 2, 3 and 4. The size of the perturbation is exaggerated greatly so that it will be visible.

The type of perturbation we expect for each mode, greatly exaggerated, is shown in Figure 2-1. Now, this perturbation will obviously produce a slight change  $\tilde{p}$  in the pressure, so that  $p = p_0 + \tilde{p}$ . Similarly, it will cause slight motion in all directions, so that we now have  $u_\phi = u_0 + \tilde{u}_\phi$ ,  $u_r = \tilde{u}_r$ ,  $u_z = \tilde{u}_z$ ; all the “twiddle” terms are of order  $\epsilon$ .

To determine the behavior of this system, we will use the Navier-Stokes equations and associated continuity equation, which describe the behavior of a fluid in terms of the velocity of the fluid flow at each point and the pressure at each point. These equations are analogous to  $F = ma$ , for Newtonian mechanics, and a requirement that mass be conserved. Viscosity is negligible because the Reynolds number,  $\text{Re} = \frac{\Omega^2 a}{\nu}$ , is very large for water at the speeds we are considering. In cylindrical coordinates, the Navier-Stokes equations are (Landau-Lifshitz p. 51):

$$\frac{\partial u_r}{\partial t} + u_r \frac{\partial u_r}{\partial r} + u_\phi \frac{\partial u_r}{\partial \phi} + u_z \frac{\partial u_r}{\partial z} - \frac{u_\phi^2}{r} = -\frac{1}{\rho} \frac{\partial p}{\partial r} \quad (2.3)$$

$$\frac{\partial u_\phi}{\partial t} + u_r \frac{\partial u_\phi}{\partial r} + \frac{u_\phi}{r} \frac{\partial u_\phi}{\partial \phi} + u_z \frac{\partial u_\phi}{\partial z} - \frac{u_r u_\phi}{r} = -\frac{1}{\rho r} \frac{\partial p}{\partial \phi} \quad (2.4)$$

$$\frac{\partial u_z}{\partial t} + u_r \frac{\partial u_z}{\partial r} + \frac{u_\phi}{r} \frac{\partial u_z}{\partial \phi} + u_z \frac{\partial u_z}{\partial z} = -\frac{1}{\rho} \frac{\partial p}{\partial z} \quad (2.5)$$

$$\frac{\partial u_r}{\partial r} + \frac{1}{r} \frac{\partial u_\phi}{\partial \phi} + \frac{\partial u_z}{\partial z} - \frac{u_r}{r} = 0 \quad (2.6)$$

It is clear that these equations are satisfied by the unperturbed flow as we have stated it; equation 2.3 simply reduces to  $-\frac{u_0^2}{r} = -\frac{1}{\rho} \frac{\partial p}{\partial r}$ , which is precisely equation 2.1, and in the rest of the equations all the terms are zero. Now let's plug in the perturbed equations. The terms of order zero in  $\epsilon$  are the unperturbed equations, and we just talked through how these equations are satisfied. The perturbation effects will be dominated by the terms of first order in  $\epsilon$ , giving us the equations:

$$\begin{aligned} \frac{\partial \tilde{u}_r}{\partial t} + \frac{u_0}{r} \frac{\partial \tilde{u}_r}{\partial \phi} - \frac{2u_0 \tilde{u}_\phi}{r} &= -\frac{1}{\rho} \frac{\partial \tilde{p}}{\partial r} \\ \frac{\partial \tilde{u}_\phi}{\partial t} + \frac{u_0}{r} \frac{\partial \tilde{u}_\phi}{\partial \phi} + \tilde{u}_r \frac{\partial u_0}{\partial r} + \frac{u_0 \tilde{u}_r}{r} &= -\frac{1}{\rho r} \frac{\partial \tilde{p}}{\partial \phi} \\ \frac{\partial \tilde{u}_z}{\partial t} + \frac{u_0}{r} \frac{\partial \tilde{u}_z}{\partial \phi} &= -\frac{1}{\rho} \frac{\partial \tilde{p}}{\partial z} \\ \frac{\partial \tilde{u}_r}{\partial r} + \frac{\tilde{u}_r}{r} + \frac{1}{r} \frac{\partial \tilde{u}_\phi}{\partial \phi} + \frac{\partial \tilde{u}_z}{\partial z} &= 0 \end{aligned} \quad (2.7)$$

To make these equations solvable, we make one further assumption about the flow parameters. Most of the variation in these parameters is  $r$ -dependent. If you are looking at two parts of the jet, one where the perturbation has slightly increased the radius and one where it has slightly decreased it, the velocity fields in the two slices should be essentially identical apart from some scale factor. The same should be true of different  $\phi$  locations at the same  $z$ . Thus, we can simply express the velocity perturbation as being a function of  $r$ , scaled by the same factor as  $\tilde{R}$  at that location. It is clear that pressure must then scale in the same way, if the N-S equations are to be satisfied for arbitrary  $\tilde{R}$ . We can make this assumption because the perturbations are relatively small and their wavelengths relatively large in comparison to the jet radius as  $\tilde{R}$  varies slowly enough that we can view the jet as being locally cylindrical

and make a scaling argument.

$$\begin{aligned}
\tilde{u}_r &= R(r) \frac{\tilde{R}}{\epsilon} \\
\tilde{u}_\phi &= \Phi(r) \frac{\tilde{R}}{\epsilon} \\
\tilde{u}_z &= Z(r) \frac{\tilde{R}}{\epsilon} \\
\tilde{p} &= P(r) \frac{\tilde{R}}{\epsilon}
\end{aligned} \tag{2.8}$$

Our equations then simplify to:

$$\begin{aligned}
R(\omega - im\Delta\Omega) - 2\Phi\Omega &= \frac{dP}{dr} \\
\Phi(\omega - im\Delta\Omega) - 2R\Omega &= \frac{im}{r}P \\
Z(\omega - im\Delta\Omega) &= ikP \\
\frac{dR}{dr} + \frac{R}{r} + \frac{im}{r}\Phi + ikZ &= 0
\end{aligned} \tag{2.9}$$

We can use the first two equations to solve for  $R$  and  $\Phi$  in terms of just  $P$ . Here I'm clearing up the notation a bit by using  $\gamma$  to denote the recurring expression  $(\omega - im\Delta\Omega)$ :

$$\begin{aligned}
R &= \frac{1}{\gamma^2 + 4\Omega^2} \left( \gamma \frac{dP}{dr} + \frac{2im\Omega}{r} P \right) \\
\Phi &= \frac{1}{\gamma^2 + 4\Omega^2} \left( -2\Omega \frac{dP}{dr} + \frac{im\gamma}{r} P \right)
\end{aligned} \tag{2.10}$$

We can plug these results, along with the expression for  $Z$  in terms of  $P$  from the third line in equation 2.9, and simplify to get:

$$r^2 \frac{d^2 P}{dr^2} + r \frac{dP}{dr} - P \left( \frac{k^2 r^2}{\gamma^2} (\gamma^2 + 4\Omega^2) + m^2 \right) = 0 \quad (2.11)$$

This is a modified Bessel differential equation. It has two solutions,  $I_n$  and  $K_n$ , the modified Bessel equations of the first and second kinds. However,  $K_n$  blows up at the axis and thus cannot be part of our solution. Thus,  $P(r)$  may be expressed in terms of some as-yet-to-be-determined constant  $C$ :

$$P(r) = CI_m \left( \frac{kr}{\gamma} \sqrt{\gamma^2 + 4\Omega^2} \right) \quad (2.12)$$

### 2.3.1 Boundary conditions

We now know the response of the fluid within the jet to a slight perturbation in the shape of the surface. The next step is to match this solution to the boundary conditions at the surface.

As mentioned before, the pressure just inside a liquid surface differs from the pressure outside by an amount dependent on the curvature of the surface; that is,

$$p|_{\tilde{R}} = p_0|_{\tilde{R}} + \tilde{p}|_{\tilde{R}} = \sigma \nabla \cdot \hat{n} + \frac{1}{2} \rho \Omega^2 (R_0 + \tilde{R})^2 \quad (2.13)$$

Following [4], we see that the normal to the surface has form:

$$\hat{n} = \frac{1}{\sqrt{\left(\frac{\partial \tilde{R}}{\partial z}\right)^2 + 1 + \left(\frac{1}{r} \frac{\partial \tilde{R}}{\partial \phi}\right)^2}} \left( -\frac{\partial \tilde{R}}{\partial z}, 1, -\frac{1}{r} \frac{\partial \tilde{R}}{\partial \phi} \right) \quad (2.14)$$

Taking the divergence of this gives us

$$\tilde{p}|_{\tilde{R}} = -\sigma \left( \frac{\tilde{R}}{R_0^2} + \frac{\partial^2 \tilde{R}}{\partial z^2} + \frac{1}{R_0^2} \frac{\partial^2 \tilde{R}}{\partial \phi^2} \right) + \frac{1}{2} \rho \Omega^2 (R_0 + \tilde{R})^2 \quad (2.15)$$

which, neglecting terms of order greater than 1 in  $\epsilon$ , yields:

$$\tilde{p}|_{\tilde{R}} = -\frac{\epsilon \sigma}{R_0^2} \left( 1 - k^2 R_0^2 - m^2 + B_0 \right) \frac{\tilde{R}}{\epsilon} \quad (2.16)$$

Here,  $B_0$  is the rotational Bond number, a dimensionless quantity equal to  $\frac{\rho \Omega^2 R_0^3}{\sigma} = \frac{\text{Rotational Inertia}}{\text{Curvature pressure}}$ . This number will become very useful to us later on, as it characterizes where the various modes may appear. Plugging in  $\tilde{p} = P(r) \frac{\tilde{R}}{\epsilon}$ , this boundary condition gives us:

$$\frac{\epsilon}{C} = \frac{\rho R_0^2 I_m}{\sigma (1 - k^2 R_0^2 - m^2 + B_0)} \quad (2.17)$$

The other boundary condition which we need to take into account is, naturally enough, that the surface should be moving out as fast as the liquid just inside the surface; that is,  $\tilde{u}_r|_{\tilde{R}} = \frac{\partial \tilde{R}}{\partial t}$ . This gives us  $R(R_0) = \epsilon(\gamma - im(\Omega + \Delta\Omega) - i\omega)$ . Again, substituting in  $R(r)$ , we find another expression for  $\frac{\epsilon}{C}$ :

$$\frac{\epsilon}{C} = \frac{1}{(\gamma - im(\Omega + \Delta\Omega) - i\omega)(\gamma^2 + 4\Omega^2)} \left( k\sqrt{\gamma^2 + 4\Omega^2} I'_m + \frac{2im\Omega}{r} I_m \right) \quad (2.18)$$

If we set these equal to each other, we get our desired dispersion relation. In terms of the dimensionless parameters  $x = kR_0$  and  $y = \frac{\gamma}{\Omega}$ , we get:

$$\frac{B_0}{(1 - x^2 - m^2 + B_0)} = \frac{1}{(y - im)(y^2 + 4)} \left( x\sqrt{y^2 + 4} \frac{I'_m \left( \frac{x}{y} \sqrt{y^2 + 4} \right)}{I_m \left( \frac{x}{y} \sqrt{y^2 + 4} \right)} + 2im \right) \quad (2.19)$$

We will always know what  $B_0$  we are dealing with, since it is simply a characterization of the rotation rate. In any physical system, all possible perturbations will be present in some form; the one that will be seen is the one that grows the fastest. Thus we can find what  $k$  the jet prefers to break up at by maximizing  $y$  with respect to  $x$  using the dispersion relation; this gives the wave number whose instability grows most rapidly and which therefore dominates the other  $k$ 's. We should note, however, that in our experiment, there is also a driving at  $\Omega_{\text{motor}}$  which does not correspond to the fastest growing mode but may appear because of this bias.

## 2.4 Consequences of Theory

By making some approximations to the value of the modified Bessel functions, it can be determined that the onset of each mode occurs at  $B_0 = m(m + 1)$ . However, this doesn't necessarily mean that as soon as we crank the rate past that critical  $B_0$  the new mode will appear; it may still be the case that one of the lower modes is more unstable than the newly introduced mode.

For example, if we have a  $B_0$  of 6.5, corresponding to a jet radius of  $\frac{3}{8}$ ", a surface tension of  $\sigma = 70 \frac{\text{dyne}}{\text{cm}^2}$ , a density of  $\rho = 1 \frac{\text{g}}{\text{cm}^3}$ , and a rotation rate of  $66 \frac{\text{rad}}{\text{s}}$ , both mode 0 and mode 2 can theoretically occur. Mode 0 is probably more unstable (that is, faster growing) here, but the vibration of the table is fairly slow, and thus imposes a perturbation of small  $k$  on the jet; the jet may be more unstable to mode 2 at such a small  $k$ .

Our theoretical investigations also show that the capillary wavelength that will be visible on a small, blocked jet depends on the rotation speed of the jet. As this rotational speed is increased, the wavelength of the stationary waves grows steadily smaller. For all rotation rates, the maximum traveling wave is one of wavelength  $2\pi R_0$ , the same as for non-rotating waves. However, whereas for unrotating jet this wavelength is only seen as a stationary wave in the limit as the jet speed goes to zero, from the rotating case we can see that the selection criteria for it is  $U = \lambda\Omega$ , where  $U$  is the speed of the jet where it is stopped. This means that very high up on

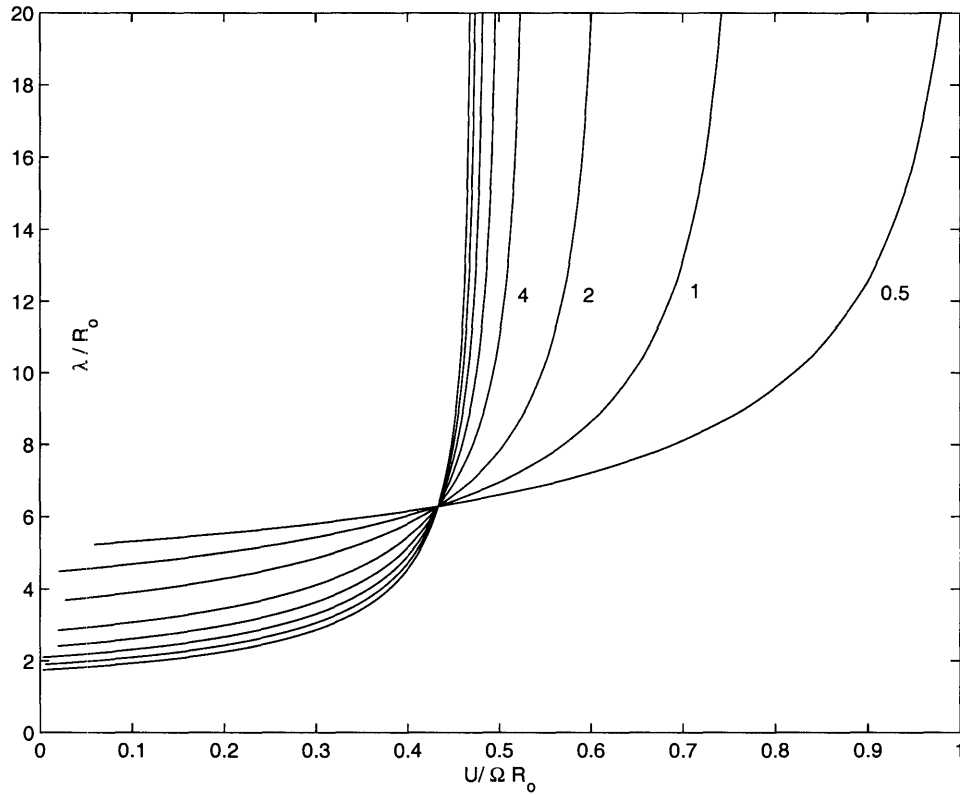


Figure 2-2: The dispersion relationship between wavelength and wave speed, for various values of  $B_0$ . Wavelengths above  $2\pi$  are not real traveling waves. Note that for some fixed value of  $U$ , that is, a fixed position on the jet, the stationary wavelength grows smaller the bigger the rotation rate  $\Omega$ .

a rotating jet, blocking the jet will produce no capillary waves, as compared to this being where waves are at a maximum for a stationary jet. The dispersion relation for various rotational bond numbers is shown in Figure 2-2.



# Chapter 3

## Experiment

There are several constraints we were trying to satisfy in the experimental design. First of all, the flow needs to be controlled enough that a clear pattern showing the target mode can be discerned under the strobe light or in a photograph, which means that we need to keep the flow as close as possible to ideal rigid body rotation up until the point where it comes out of the outlet. We also need to be able to determine exactly the cutoff rotation rate at which the various modes first appear. Therefore, the rotation rate must be precisely measurable.

A diagram and photograph of the experimental setup are shown in Figure 3-1. The jet falls into a large tank of water, from which water can be pumped at an adjustable rate into the rotating tank at the top. This tank sits on a turntable that is driven by a motor that can drive the table up to about 18 Hz. There is also a lower limit in the useful speeds; below about 1 Hz the table's momentum is insufficient to keep it rotating smoothly, and the motor's power is somewhat low, with the effect that the table turns in a lurching fashion rather than smoothly. The joint between the feed line and the rotating tank is freely rotating and magnetically sealed; thus it can be cracked open temporarily to let air out so that the upper tank can be filled.

The pump pressure can be varied from barely enough to support siphon flow through the tank, to some pressure and corresponding flux rate dependent on the size of the outlet nozzle; above this rate either the pump can't supply enough pressure or the magnetic seal will open and let the tank leak. The fact that there's an upper

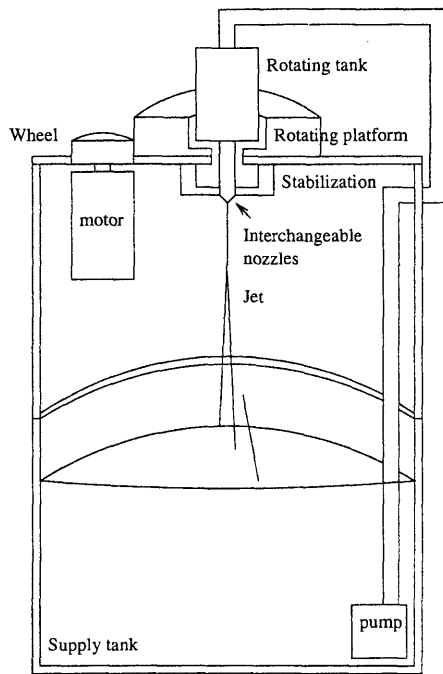


Figure 3-1: The experimental setup. A pump feeds water from the large reservoir into a small drum which can be rotated reliably at any speed from 1 to 18 Hz. This water then exits through any of a number of interchangeable nozzles. The jet can be seen more clearly using a strobe light.

limit on the pump pressure means that the upper tank won't spontaneously explode, although the turntable will still fling water at the experimenters if they go above the pressure limit and the seal opens. The limit for the  $\frac{3}{8}$ " nozzle, for example, is set by the pump power, and is about  $140\text{-}160 \frac{\text{mL}}{\text{s}}$ , much faster than anything we need.

The motor has a tachometer accurate to within about .01 Hz of table-speed. The rate of flow may be measured simply by directing the jet into a graduated cylinder for a set number of seconds, and does not vary significantly with time. The available nozzles range in size from  $\frac{1}{4}$ " to  $\frac{1}{2}$ ", in increments of  $\frac{1}{16}$ ".

To make sure that the jet is originally in laminar flow and solid-body rotation, the entrance to each nozzle is packed with wire mesh. As the flow enters the nozzle, its extra angular momentum (vorticity, in fluid dynamics terms) is converted into turbulence, which, dying off, leaves solid-body rotation at a new rate and shape; the wire mesh helps the water jet spin up to the rotation rate of the nozzle faster.

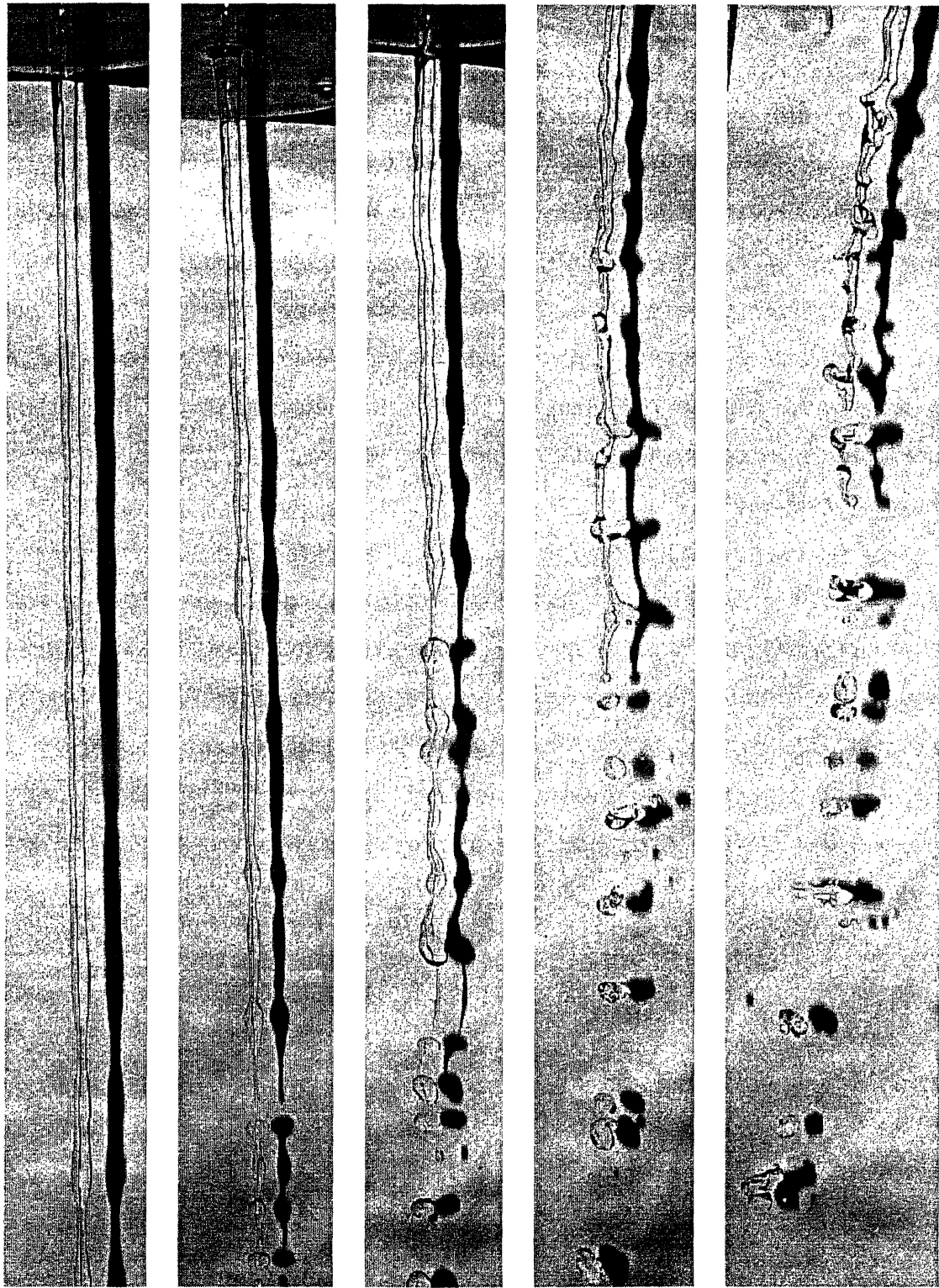
In a typical experimental run, we fill the upper tank, then close its seal and run

the pump near the maximum flux for a while until all the residual bubbles are forced out of the rotating tank; then we can sweep through a variety of pressure and rotation rate settings, first trying to image the instability by matching the strobe frequency to the breakup frequency, and then taking a photograph. We pay more attention to rotation rates close to a mode change, trying to pin down where the transitions occur, but there are also less major variations that occur within a mode.

Changing the nozzle requires removing the rotating tank, applying new adhesive around the nozzle, and waiting for it to dry; thus, this is done in between runs. We can get a good seal by simply using silicone grease around the nozzle, but this also lubricates it, giving the nozzle a tendency to be ejected due to pressure in the tank during the experiment.

One interesting feature of our experimental setup is that the jet is being strongly driven at the  $k$  of the motor. Thus, rather than breaking up at its most unstable wavelength, the jet may try to break up at the motor's frequency, if that frequency is in the right range. The motor's frequency is higher than the  $\Omega$  of the table by a factor of 2.22; thus, the jet has a strong bias toward breaking up at  $k = \frac{U_{outlet}}{\Omega}$ .

Pictures from an experimental runs are shown in figures 3-2, 3-3, and 3-4. In this run, the nozzle size is .95 cm, and the pump pressure is just enough to replenish the tank.



$B_0 = 0$   
 $\Omega = 0\text{Hz}$

$B_0 = 0.21$   
 $\Omega = 1.88\text{Hz}$

$B_0 = 0.85$   
 $\Omega = 3.76\text{Hz}$

$B_0 = 1.92$   
 $\Omega = 5.63\text{Hz}$

$B_0 = 3.41$   
 $\Omega = 7.51\text{Hz}$

Figure 3-2: A sequence showing the water jet breakup as rotation rate increases, for a jet radius  $R_0 = .95\text{cm}$ . Note that the mode 0 instability first starts to grow more rapidly and to segment off smaller, ellipsoidal drops

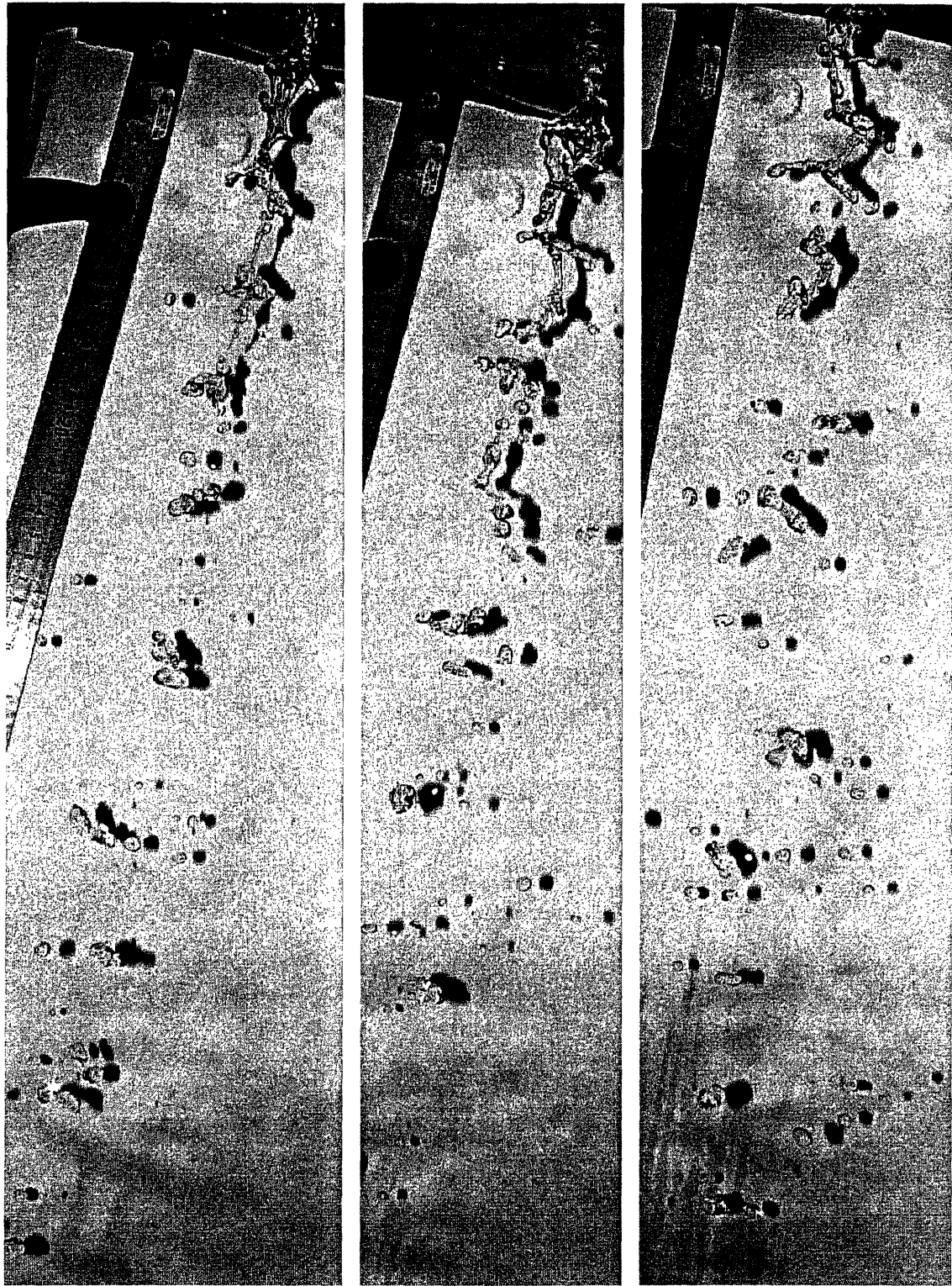


$B_0 = 5.33$

$B_0 = 7.67$

$B_0 = 10.44$

Figure 3-3: As the rotation rate increases, mode appears (middle) and grows progressively more unstable. Jet radius here is still  $R_0 = .95\text{cm}$ . The individual drops, rather than consolidating back into a drop under the influence of surface tension as their rotation rate slows, instead are torn apart into two main drops, usually leaving some daughter drops as well where the connecting bar was.



$B_0 = 13.64$

$B_0 = 17.26$

$B_0 = 19.64$

Figure 3-4: At fairly high rotation rates, mode 2 instabilities develop immediately and the jet breaks up almost as soon as it leaves the nozzle. Mode 3 may be visible in the final picture.



# Chapter 4

## Results

### 4.1 Experimental Results

At the moment, we are still collecting results from the experiment. One fairly successful trial run with a  $\frac{3}{8}$ " jet showed breakup starting near  $B_0 = 5.3$  for mode 2, which is at least somewhat close to what the theory suggests. However, this is not nearly close enough to make us happy, especially since it is short of the cutoff below which mode 2 is not supposed to appear at all. It is possible that we did not measure the parameters of the system with enough accuracy, or that our water reservoir, which has been standing out in the lab for weeks, is contaminated with something that reduced its surface tension. Water standing in the open tends to have a surface tension  $60 \frac{\text{dyne}}{\text{cm}^2} < \sigma < 70 \frac{\text{dyne}}{\text{cm}^2}$ .

In the course of running the experiment for which pictures are shown here, the motor skook loose a small screw on its side, allowing a bushing held by that screw to fall inside the motor case. When we started the next experimental run, trying to pin dwn more exactly the critical  $B_0$  for the second mode, this bushing was drawn into the motor and rattled around for a few seconds before I yanked the plug. After clearing it from the motor by rotating the shaft manually, I ran the motor again, heard no rattling, and had just happily concluded that no damage was done, when I looked up and saw the motor enveloped in a cloud of smoke. Thus, we are waiting on repairs to our motor before we can get more precise results, or investigate the

behavior of capillary waves on a small jet.

Theoretically, since the rotational Bond number is the only parameter that matters when we ignore the effects of gravity, one nozzle size is sufficient to determine the cutoff points; however, we intend to try a wide variety of sizes to ensure that the gravity effects are in fact sufficiently small to be neglected.

## 4.2 Contributions

In this paper, we have:

- Derived the conditions under which a rotating jet is unstable to various modes of instability, critical rotational Bond numbers  $B_0$ .
- Shown that experimental results agree qualitatively with theory.
- Described qualitatively the jet evolution within each mode.

These results add to a growing body of information on surface-tension-driven instabilities of fluid flows. Most of the nonrotating flows have been solved long enough ago to become textbook examples, but the instabilities of rotating fluids in configurations such as drops, jets, and vortices still provide a wealth of open questions.



# Bibliography

- [1] Gregory J. Balle. Break-up of a slowly rotating water jet. *Washington University Ocean 569 Lab Final Report*, March 1999.
- [2] R. A. Brown and L. E. Scrivens. The shape and stability of rotating liquid drops. *Proceedings of the Royal Society of London, Series A*, 371(1746):331–357, June 1980.
- [3] John Bush. Lecture notes on jet instabilities. (Jet shape, Rayleigh-Plateau instability, fluid pipes).
- [4] P. G. Drazin and W. H. Reid. *Hydrodynamic Stability*, chapter 1, pages 1–27. Cambridge University Press, 1981.
- [5] Linda T. Elkins-Tanton, Pascale Aussillous, Jose Bico, David Quere, and John W. M. Bush. A laboratory model of splash-form tektites. *Meteoritics & Planetary Science*, 38(9):1331–1340, 2003.
- [6] Matthew J. Hancock and John W. M. Bush. Fluid pipes. *Journal of Fluid Mechanics*, 466:285–304, 2002.
- [7] Horace Lamb. *Hydrodynamics*, chapter 12. Cambridge University Press, New York, 1993.
- [8] J. Plateau. *Statique Experimentale et Theorique des Liquides Soumis aux Seules Forces Moleculaires*. GauthierVillars, Paris, 1873.
- [9] Lord Rayleigh. On the instability of jets. *Proc. Lond. Math. Soc.*, 10:4–13, 1879.

- [10] Lord Rayleigh. On the stability of a cylinder of viscous liquid under capillary force. *Phil. Mag.*, 34:145–154, 1892.
- [11] D. F. Rutland and G. J Jameson. Droplet production by the disintegration of rotating liquid jets. *Chemical Engineering Science*, 25:1301–1317, 1970.
- [12] Nikos Savva. Stability of a rotating jet. (Notes from PhD thesis (in preparation)).